Triple oxygen and hydrogen isotopes of gypsum hydration water for quantitative paleo-humidity reconstruction

Fernando Gázquez[1*], Mario Morellón[2], Thomas Bauska[1], Daniel Herwartz[3], Jakub Surma[3], Ana Moreno[4], Michael Staubwasser[3], Blas Valero-Garcés[4], Antonio Delgado-Huertas[5] and David A. Hodell[1]

[1]*Godwin Laboratory for Palaeoclimate Research. Department of Earth Sciences. University of Cambridge. Downing Street, Cambridge, CB2 3EQ, United Kingdom*

[2]*CITIMAC, Facultad de Ciencias. University of Cantabria. Avenida de los Castros s/n, 39005, Santander, Spain*

[3]*Institute für Geology und Mineralogy. Universität zu Köln. Greinstrasse. 4-6, 50939, Köln, Germany.*

[4]*Department of Environmental Processes and Global Change, Pyrenean Institute of Ecology (IPE) – CSIC, Campus de Aula Dei, Avenida Montañana, 1005, E-50059, Zaragoza, Spain.*

[5]*Laboratorio de Biogeoquímica de Isotopos Estables, Instituto Andaluz de Ciencias de la Tierra IACT (CSIC-UGR). Avda. de las Palmeras, 4, 18100, Armilla, Granada, Spain*

*now at *School of Earth and Environmental Sciences. University of St. Andrews. St Andrews, KY16 9AL, Scotland, United Kingdom.*

Abstract

Atmospheric relative humidity (RH) is an important parameter affecting vegetation yet palaeo-proxies for RH are scarce and difficult to calibrate. Here we use triple oxygen ($\delta^{17}O$ and $\delta^{18}O$) and hydrogen (δD) isotopes of structurally bounded gypsum hydration water (GHW) extracted from lacustrine gypsum to quantify past changes in paleo-atmospheric RH. An evaporation

isotope mass balance model is used together with Monte Carlo simulations to determine the range of climatological conditions that simultaneously satisfy the stable isotope results of GHW, and with statistically robust estimates of uncertainty. We apply this method to reconstruct the isotopic composition of paleo-waters of Lake Estanya (NE Spain) and changes in atmospheric RH over the last glacial termination and Holocene (from ~15 to 0.6 cal. kyrs BP). The isotopic record indicates the driest conditions occurred during the Younger Dryas (YD; ~12-13 cal. kyrs BP). We estimate a RH of ~40-45% during the YD, which is ~30-35% lower than today. Because of the southward displacement of the Polar Front to ~42^{o}N, it was both windier and drier during the YD than the Bølling-Allerød period and Holocene. Mean atmospheric moisture gradually increased from the Preboreal to Early Holocene (~11 to 8 cal. kyrs BP, 50-60%), reaching 70-75% RH from ~7.5 cal. kyrs BP until present-day. We demonstrate that combining hydrogen and triple oxygen isotopes in GHW provides a powerful tool for quantitative estimates of past changes in relative humidity.

Keywords: triple oxygen isotopes, gypsum hydration water, relative humidity, lake sediments, Younger Dryas, Late Glacial-Holocene transition.

1. Introduction

The presence of gypsum ($CaSO_4 \cdot 2H_2O$) in lacustrine sediments is commonly interpreted as evidence of dry climatic conditions in the past (Hodell et al., 1995, 2005; 2012; Torfstein et al., 2008; Morellón et al., 2009a; Escobar et al., 2012, amongst many others). Evaporation of Ca^{2+}-SO_4^{2-}-rich lake waters can lead to gypsum supersaturation under conditions of high evaporation relative to precipitation (inflow). These conditions are generally accompanied by decreased input

of fine-grained allochthonous sediments as a result of decreasing runoff, resulting in sediments that are dominantly composed of gypsum. Interbedded layers of gypsum and other "non-evaporitic" facies in lakes are often attributed to alternating wet and dry conditions (e.g. Hodell et al., 1995; Ortiz et al., 2006; Morellón et al., 2009a; Escobar et al., 2012; Valero-Garcés et al., 2014; Li et al., 2017).

The isotopic composition of lake waters is sensitive to long-term changes in the Evaporation/Inflow (E/I) regime and atmospheric relative humidity (RH), among other parameters (Gibson et al., 2016). In addition to E/I and RH, climatic variations recorded in lacustrine carbonates (i.e. $\delta^{18}O$ of authigenic carbonates) can be masked by the effect of temperature on the oxygen isotopic value during carbonate precipitation (Hodell et al., 2012). In contrast, structurally bounded gypsum hydration water (GHW) can be used to reconstruct the isotopic value of paleo-lake waters with little to no effect of temperature. The fractionation factors for oxygen and hydrogen isotopes between the free solution and GHW are largely independent of temperature in the range of most lakes (e.g. 10-35^{o}C; Gázquez et al., 2017a). Thus, the oxygen and hydrogen isotopes ($\delta^{18}O$ and δD) of GHW can be used to infer the isotopic composition of paleo-lake waters at the time of gypsum precipitation (Hodell et al., 2012; Grauel et al., 2016; Li et al., 2017). GHW retains the isotopic values of the parent solution provided that it has not been altered by post-depositional processes (e.g. exposure to temperature >50^{o}C after deposition, solution-reprecipitation, etc.). Whether the original isotopic composition of GHW has been preserved or not must be evaluated on a case-by-case basis (Hodell et al., 2012; Evans et al., 2015; Gázquez et al., 2017a).

Recent analytical developments permit precise measurements of triple oxygen isotopes ($^{17}O/^{18}O/^{16}O$), and the derived parameter ^{17}O-excess (also called $\Delta^{17}O$), in natural waters (Luz

and Barkan, 2010; Steig et al., 2014) and GHW (Gázquez et al., 2015) with precision better than ±0.01‰ (i.e. 10 per meg; ±1σ). This parameter is defined as:

$$^{17}\text{O-excess} = \ln(\delta^{17}\text{O} + 1) - 0.528 \ln(\delta^{18}\text{O} + 1) \quad \text{(Eq. 1)}$$

where:

$\delta^{17}O$ and $\delta^{18}O$ denote the $^{17}O/^{16}O$ and $^{18}O/^{16}O$ in water standardized to V-SMOW (Barkan and Luz, 2005; Luz and Barkan, 2010; Schoenemann et al., 2013). The value of 0.528 has been proposed to describe the $\delta^{17}O$ and $\delta^{18}O$ relationship in rainwater worldwide (Luz and Barkan, 2010). The ^{17}O-excess averages ~37 per meg in modern meteoric waters and shows lower values in evaporated water (Barkan and Luz, 2010; Steig et al., 2014; Surma et al., 2015). The trajectory of $\delta^{18}O$ and ^{17}O-excess in evaporated water is relatively insensitive to temperature and salinities below 100 g/l (Barkan and Luz, 2010; Passey et al., 2014); however, it is significantly affected by other parameters such as the hydrological balance of the water body and atmospheric RH (Surma et al., 2015; Gázquez et al., 2017b; Herwartz et al., 2017; see Fig. 1).

Despite the potential of lake sediments as palaeoclimatic archives, stable isotopes in inorganic and organic proxies often allow only qualitative interpretation of past hydrological changes. Quantitative reconstructions from isotope proxy data, including changes in atmospheric relative humidity, have been difficult to achieve and calibrate. Here we evaluate the potential of using triple oxygen and hydrogen isotopes in lacustrine GHW to quantify changes in atmospheric relative humidity in the past. We use a Raleigh evaporation isotope mass balance (IMB) to estimate quantitatively climatic conditions at the time of gypsum precipitation. Monte Carlo simulations are used to find the most probable solution to the model and evaluate uncertainties for RH. We apply this method to isotopic data ($\delta^{17}O$, $\delta^{18}O$ and δD, and derived d-excess and ^{17}O-excess) of gypsum hydration water from Lake Estanya (Southern Pre-Pyrenees, NE Spain)

to infer climate during the Late Glacial and Holocene periods (ca. 15 cal. kyrs BP to 0.6 cal. kyrs BP). We model the isotopic values of paleo-lake Estanya under different environmental/geochemical scenarios. We compare the isotopic results and derived RH values with previous sedimentological and geochemical proxies in the lake sequence (Morellón et al., 2009b), as well as other biological indicators such as pollen, diatoms and chironomids (Morellón et al., 2011; Vegas-Vilarrùbia et al., 2013; González-Sampériz, 2017). Lastly, we discuss more generally the potential application of the method to other lakes.

2. Approach and model

The oxygen ($\delta^{17}O$ and $\delta^{18}O$) and hydrogen (δD) isotopic composition of lake waters increase with more arid conditions and higher evaporation relative to inflow (E/I). Each isotope ratio follows a slightly different fractionation leading to variability in d-excess and ^{17}O-excess parameters (Surma, 2015; Gibson et al., 2016; Herwartz et al., 2017; and references therein). The isotopic evolution of water during evaporation (e.g. $\delta^{18}O$ vs ^{17}O-excess and $\delta^{18}O$ vs d-excess) depends on the isotopic composition of the initial water (inflow), temperature, relative humidity, the isotopic composition of the water vapor in equilibrium with the liquid water and the ratio of water loss by evaporation (E) with respect to the inflow (I), with the remainder lost as outflow. The process is described by the expression (Criss, 1999):

$$ {}^{*}R_{WS} = \frac{{}^{*}\alpha^{0}_{evap} \cdot (1-h) \cdot {}^{*}R_{WI} + {}^{*}\alpha^{0}_{eq} \cdot h \cdot E/I \cdot R_V}{E/I + {}^{*}\alpha^{0}_{evap} \cdot (1-h) \cdot (1-E/I)} \quad \text{(Eq. 2)} $$

Where $*R_{WS}$ is the isotopic ratio of the evaporated water. $*\alpha^0_{evap}$ is the effective fractionation factor, calculated as a product of the equilibrium fractionation factor ($*\alpha^0_{eq}$) and the diffusive fractionation factor ($*\alpha^0_{diff}$) between the liquid water and vapor. The parameter *h* is the relative humidity of air (0 to 1). R_{WI} is the isotopic ratio of the input prior to evaporation (i.e., the inflow to the lake). R_v is the isotopic ratio of the vapor and depends on the degree to which the atmospheric water vapor (v_{eq}) is in equilibrium with R_{WI} (Gibson et al., 2016), where:

$$R_v = R_{WI} * (\alpha^0_{eq} * v_{eq}) \quad \text{(Eq. 3)}$$

E/I represents the fraction of water loss by evaporation with respect to the inflow from the system (e.g. E/I =0 means no evaporation whereas E/I =1 means all the water is lost to evaporation; i.e. there is no outflow). This model assumes homogeneous isotopic composition of both the liquid and vapor phases.

Equilibrium fractionation factors for $\delta^{18}O$ and δD are well known and calculated here as a function of temperature using the equations of Horita and Wesolowski (1994). $\alpha^{17}O^0_{eq}$ is calculated as $\alpha^{17}O^0_{eq} = \alpha^{18}O^{0\,\theta}_{eq}$, where θ is 0.529 (Barkan and Luz, 2005). Kinetic fractionation during evaporation under natural conditions is not as strongly constrained as equilibrium fractionation. Here we use a combination of natural and laboratory experiments to calculate α^0_{diff} (Landais et al., 2006; Barkan and Luz, 2007, Luz et al., 2009). First, $\alpha^{18}O^0_{diff}$ varies as a function wind driven turbulence (Dongmann et al., 1974; Uemura et al., 2010; Haese et al., 2013) (see discussion section) and is calculated as:

$$\alpha^{18}O^0_{diff} = 1.0283^w \quad \text{(Eq. 4)}$$

where *w* varies between 0.5 (pure turbulent mixing; $\alpha^{18}O^0_{diff} = 1.0141$) and 1.0 (pure diffusion; $\alpha^{18}O^0_{diff} = 1.0283$).

136 αD^0_{diff} varies as a function of $\alpha^{18}O^0_{diff}$ and temperature (T, in ^oC) based on experiments by Luz
137 et al. (2009), where:

138 $$\alpha D^0_{diff} = (1.25\text{-}0.02\ T)\ (\alpha^{18}O^0_{diff}\text{-}1) + 1 \quad \text{(Eq. 5)}$$

139

140 $\alpha^{17}O^0_{diff}$ is calculated as $\alpha^{17}O^0_{diff} = \alpha^{18}O^0_{diff}{}^{\theta}$, where θ is 0.5185 (Landais et al., 2006; Barkan
141 and Luz, 2007).

142 In $\delta^{18}O$-^{17}O-excess and $\delta^{18}O$-d-excess space (Fig. 1), the predicted trends of waters undergoing
143 evaporation in partial equilibrium with atmospheric vapor take the form of curves. We see that
144 both ^{17}O-excess and d-excess are largely sensitive to RH during evaporation (Fig. 1A and F),
145 whereas their sensitivities to temperature are relatively small, especially for ^{17}O-excess (Fig. 1B)
146 (Landais et al., 2006; Passey et al., 2014; Surma et al., 2015; Gázquez et al., 2017b; Herwartz et
147 al., 2017). Both cross-plots are moderately sensitive to turbulences (winds) on the water surface
148 during evaporation (Fig. 1C and H) and to the isotopic composition of the atmospheric water
149 vapor (Fig. 1D and I). Also, both isotopic systems are very sensitive to the proportion of water
150 loss by evaporation with respect to the input (E/I) (Fig. 1E and J).

151 In summary, our isotopic model is based on three equations where $\delta^{17}O$, $\delta^{18}O$ and δD are known
152 (measured), four variables that can be constrained by modern estimates ($\delta^{17}O$, $\delta^{18}O$ and δD of
153 the inflow and lake temperature), two poorly constrained but minor variables (turbulence and
154 vapor-precipitation equilibrium) and two significant unknowns (E/I and h). Estimating E/I and h
155 in the past requires some assumptions about the errors in the unknown variables and an
156 understanding of how these variables co-vary and introduce uncertainty in the model results (see
157 discussion section).

158

159 Monte Carlo simulations performed in Matlab® is used in our method to find the possible model
160 solutions that satisfy the isotopic composition of the modern and paleo-lake water given the
161 uncertainty in both the paleo-environmental parameters considered and the analytical errors. The
162 approach is represented graphically in Figure S3. Briefly, a range of model inputs is selected
163 based on conservative estimates of their distributions in the modern and potential to change in
164 the past. The distribution of model inputs is uniform and thus produces a largely uniform set of
165 model solutions. The error in each model solution is then calculated relative to the mean and 1-
166 sigma standard deviation (1SD) of each individual data point. The normalized errors for $\delta^{18}O$,
167 δD, and ^{17}O-excess are then combined to arrive at a total error (if no ^{17}O-excess data exists it is
168 excluded from the total error). Only those model solutions that fall within the 1SD are then
169 selected. In the three-dimensional space of the $\delta^{18}O$, δD, ^{17}O-excess, this can be visualised as
170 selecting all the data points that fall within an ellipsoid with axes that extend to the 1SD
171 analytical error in each parameter. From the subset of simulations, the mean and range of model
172 inputs (e.g. relative humidity) that are constituent with the lake water isotopes can derived.

173

174 **3. Materials and methods**

175 Balsas de Estanya is a karstic lake complex located at the foothills of the Southern Pyrenees
176 (42º02'N, 0º32'E) at 670 m a.s.l. It is a relatively small endorheic basin of 2.45 km^2 (Fig. 2) that
177 comprises multiple bodies of water. The largest and deepest lake (Estanque Grande de Abajo)
178 has been studied extensively for paleoclimate and paleolimnological reconstruction (Morellón et
179 al., 2009b; 2011; and references therein) (Fig. 2 and supplementary material). Twenty-nine
180 gypsum samples were collected from the ca. 11-m long composite sequence of Lake Estanya,
181 which is comprised of a combination of cores LEG04-1A-1K and EST06-1A-1U (Morellón et

al., 2009b). The cores were recovered from the deepest areas of Estanque Grande de Abajo (Fig. 2). The age model is based on radiocarbon, ^{137}Cs and ^{210}Pb and lithostratigraphy as previously described by Morellón et al., (2009b) and Vegas-Vilarrùbia et al. (2013) (see supplementary material).

GHW was extracted by heating the powdered gypsum *in vacuo* using a bespoke offline system consisting of six vacuum lines contained within a modified gas chromatography (GC) oven in the Godwin Laboratory at the University of Cambridge (UK) (Gázquez et al., 2015). Oxygen ($\delta^{17}O$ and $\delta^{18}O$) and hydrogen (δD) isotopes of the hydration water were measured simultaneously by cavity ringdown spectroscopy (CRDS) using a L2140-i Picarro water isotope analyzer (Gázquez et al., 2015 and supplementary material for details). All results are reported in parts per thousand (‰) relative to V-SMOW. The uncertainty of the method was ±0.05‰ for $\delta^{17}O$, ±0.1‰ for $\delta^{18}O$ and ±0.6‰ for δD, ±0.8‰ for d-excess and ±8 per meg for ^{17}O-excess (1SD).

Additionally, the hydration water of two samples were also analyzed for $\delta^{17}O$ and $\delta^{18}O$ using a modified version of the fluorination-IRMS method of Barkan and Luz (2005) at the Institute for Geology and Mineralogy at the University of Cologne, Germany (Surma et al., 2015; Gázquez et al., 2015; Herwartz et al., 2017). Rain (n=59) and lake waters (n=61) collected between 2001 and 2012 were analyzed for oxygen and hydrogen stable isotopes (Tables S2, S3, S4 and S5 in supplementary material).

4. Results

Twenty-nine gypsum samples, ranging in age from 14.7 to 0.6 cal. kyrs BP, were analyzed for stable isotopes in GHW. The $\delta^{17}O$ varies from 3.8‰ to 7.1‰, $\delta^{18}O$ from 6.3‰ to 14.9‰ and δD from −26.1‰ to 3.0‰ (Table S1 and Fig. S2 in supplementary material). The lowest values

correspond to gypsum samples at 136 cm below lake floor; ca. 620 cal. yr BP) and the highest values to gypsum at 588 cm depth; ~12 cal. kyrs BP).

The oxygen and hydrogen isotope composition of the parent water from which the gypsum formed is calculated from GHW using recently revised fractionation factors ($\alpha_{gypsum\text{-}water}$) (Gázquez et al., 2017a) that are more precise and accurate than previous values (Gonfiantini and Fontes, 1963; Fontes and Gonfiantini, 1967; Hodell et al., 2012). We use $\alpha^{18}O_{gypsum\text{-}water}$ of 1.00355 and $\alpha D_{gypsum\text{-}water}$ of 0.979 corresponding to a temperature of 15^{o}C, representing roughly the modern mean temperature of the lake water (~12.5^{o}C). Note that both, $\alpha^{18}O_{gypsum\text{-}water}$ and $\alpha D_{gypsum\text{-}water}$ are largely unaffected by temperature in the range from 10^{o}C to 35^{o}C (Gázquez et al., 2017a). The use of temperatures that are 10^{o}C higher or lower changes the $\delta^{18}O$ values by only ~±0.1‰ and δD by ~±2‰, which is not very significant relative to the analytical precision of our method.

The relation between $\alpha^{17}O_{gypsum\text{-}water}$ and $\alpha^{18}O_{gypsum\text{-}water}$ is given by the parameter θ ($\alpha^{17}O_{gypsum\text{-}water} = \alpha^{18}O_{gypsum\text{-}water}{}^{\theta}$), which has been found to be 0.5297±0.0012 and does not depend on temperature between 3 and 55^{o}C (Gázquez et al., 2017a). Therefore, we use $\alpha^{17}O_{gypsum\text{-}water}$ of 1.00188. Using these alpha values, we found that the paleo-lake water (i.e., GHW corrected for fractionation) plot on an evaporation line with slope of 3.4 (Fig. 3). This evaporation line is comprised of paleo-lake waters from different ages that evaporated under different environmental conditions. Therefore, the slope of this line does not convey a unique paleo-hydrological significance.

From 14.7 to 13.3 cal. kyrs BP during the Bølling-Allerød (B-A) period, the $\delta^{18}O$ values of the lake water increased gradually from 7.8‰ at 14.7 cal. kyrs BP to 10.6‰ at 13.3 cal. kyrs BP, while δD increased from 12.1‰ to 21.9‰. During the same period, d-excess varied from -

50.4‰ to -62.6‰. The $\delta^{18}O$ and δD of the lake water shows the highest values of the entire record at ca. 12 cal. kyrs BP (11.3‰ and 23.7‰, respectively) during the Younger Dryas (YD) Chronozone. This time also marked the lowest d-excess values (-69‰) (Table S1). During the following Preboreal-Holocene period (from 11.7 to 7.5 cal. kyrs BP), $\delta^{18}O$ and δD values decreased to ~5.5‰ and ~2.4‰, respectively. Finally, the isotopic composition of the lake water reached full Holocene conditions after ~7.5 cal. kyrs BP ($\delta^{18}O$ of 4.3±0.7‰ and δD of -1.5±2.9‰), showing similar values to modern Lake Estanya water ($\delta^{18}O$ of 3.6±0.7‰ and δD of -2.4±7.1‰). The ^{17}O-excess of paleolake water during the Holocene ranged from -63 to -46 per meg, also resembling modern values (-51 per meg). More negative ^{17}O-excess values were recorded during the Preboreal-Early Holocene (-103 to -94 per meg), the YD (-82 per meg) and the B-A period (-67 per meg).

5. Discussion

5.1. Reliability of GHW results

Recent stable isotope studies of GHW in lakes have produced relevant paleoclimatic records that closely agree with other local and regional climatic proxies (Hodell et al., 2012; Grauel et al., 2016; Li et al., 2017 and the present study). Such excellent correlations undoubtedly indicate that, at least in some cases, the primary isotopic composition of GHW is preserved in time. Investigations on Messinian gypsum deposits (ca. 5.9 Ma) also suggest no isotopic exchange or alteration of the primary isotopic signal (Evans et al. 2015). However, it must be considered that in other sedimentary sequence, GHW may have undergone isotopic modification, for example by dehydration/rehydration cycles as a result exposure of gypsum to temperature >50^{o}C (e.g. burial

and exhumation cycles). Therefore, the reliability of stable isotopes in GHW to reconstruct the isotopic composition of paleo-waters should be evaluated on a case-by-case basis.

There are several lines of evidence that GHW in Lake Estanya preserves its primary isotopic signature. After applying fractionation factors, the values of the Mid- Late-Holocene paleolake waters roughly match the modern lake water; however, the Early Holocene and Late Glacial paleolake waters (~7.5 to ~15 cal. kyrs BP) show considerably more enriched values. If the GHW had exchanged with sediment pore water, we would expect a relatively homogeneous isotopic profile with values similar to the current lake water. Because the burial depth is shallow and sediments are porous we expect any isotopic gradients in pore water to be strongly attenuated by diffusion and advection with overlying lake water.

The isotopic changes in GHW through the late Glacial-Holocene transition and the Holocene strongly correlate with major climatic changes recorded by other regional and local paleoclimate archives, including several sedimentary proxies in Lake Estanya. Accordingly, we suggest the hydration water of gypsum deposits in Lake Estanya reflects the isotopic composition of the paleo-lake water during the latter part of the last deglaciation and Holocene.

5.2. Determining RH from isotopic analysis of GHW

The ability of GHW to record the isotopic composition of the original fluid, with little to no effect of temperature, makes it a near direct proxy for the isotopic composition of paleowater. The method presented here permits $\delta^{17}O$, $\delta^{18}O$ and δD, and derived d-excess and ^{17}O-excess to be determined simultaneously in the same sample. The isotopic composition of paleo-lake water can then be used to model the hydrologic parameters of the basin and climatic conditions at the time of gypsum precipitation. Importantly, the ability of this method to reconstruct the ^{17}O-

excess of paleo-waters, which is dependent of RH and practically insensitive to temperature during water evaporation, constitutes a powerful tool for paleo-hydrologic reconstructions.

When modelling the isotopic composition of paleo-lakes to fit the GHW data, several parameters must be known or assumed. The uncertainty in some variables, including temperature and the isotopic composition of the freshwater member, have relatively little effect on the results of the model (Fig. 4 and 5B). For example, a temperature change of 3-5^{o}C, as expected for the last Glacial-Holocene transition in some regions (see section 5.3), barely affects the model results for ^{17}O-excess (up to ~±2 per meg in a terminal lake), whereas d-excess changes by up to ~3‰ in a terminal lake, when keeping all other parameters constant. Importantly, the model solution must satisfy both ^{17}O-excess and d-excess of the same paleo-water.

The isotopic composition of rainfall varied between glacial and interglacial periods in most regions, as recorded by speleothems, paleo-groundwaters and ice cores. For example, δ^{18}O of freshwater in the western-Mediterranean region increased up to ~1‰, although practically no change has been observed in south Iberia during the last glacial-Holocene transition (Jasechko et al., 2015) (see section 4.2. in supplementary material). As seen in Fig. 5B, when keeping other parameter constant, a 1‰ change in δ^{18}O of the input will result in uncertainties of 3 to 4.6% in the modeled RH. However, it worth noting that larger change in δ^{18}O of the rainfall may be expected in other regions; for example, in areas affected by monsoonal systems and large variations in the “amount effect” over glacial-interglacial cycles (e.g. southern Asia; Kathayat et al., 2016). Therefore, uncertainties in the isotopic composition of the freshwater member must be considered as a potential source of error for quantitative paleo-humidity estimates when using this method.

294 The isotopic composition of the modern atmospheric vapor and how it varies with time is
295 unknown in most regions, nor there are estimates available for this parameter in the past.
296 However, a recent study suggests that the isotopic composition of atmospheric vapor is often in
297 partial equilibrium with that of local freshwater. A degree of equilibrium of 75% seems
298 reasonable for most tropical and intertropical regions (Gibson et al., 2016). Our IMB model does
299 not reproduce the measured $\delta^{18}O$, $\delta^{17}O$ and δD ratios for any reasonable set of input parameters
300 when full equilibrium is assumed. The model is relatively sensitive to the isotopic composition
301 of the vapor, as shown in Fig 1D. This must be considered when modeling the isotopic
302 composition of lakes in coastal areas that can be affected by advection of marine air masses,
303 whose isotopic composition is in equilibrium with seawater instead of freshwater.

304 The effect of turbulence (e.g., wind) on the isotopic equilibrium between water and vapor is
305 accounted for in our model by replacing $*\alpha_{diff}$ by $(*\alpha_{diff})^{w}$, where the exponent 'w' is set between
306 0.5 (pure turbulence) and 1 (no wind) (Dongmann et al., 1974; Uemura et al., 2010; Haese et al.,
307 2013). The relationship between this parameter and the wind speed is not well constrained;
308 however, it is known that the proportion of $*\alpha_{diff}$ may be suppressed by turbulent flow induced
309 by wind (e.g. Horita et al. 2008). As exemplified in Fig. 4 (see section 5.3 and supplementary
310 material for details), when turbulence is not considered, the model yields d-excess and ^{17}O-
311 excess values that are systematically too low compared to the analytical data for some periods
312 (i.e. Younger Dryas; ~12 ka). This offset can be corrected by reducing the value of the exponent
313 'w' for periods that are documented to have been windier than the average.
314 The hydrologic balance of the lake (E/I) controls the isotopic composition of the water. Lakes
315 with high E/I values (i.e. lakes of dry regions) may also show high salinities due to accumulation
316 of salts in the basin. However, the salt effect on the IMB becomes significant only at >100 g/l

(Sofer and Gat, 1972; Criss 1999; Herwartz et al., 2017). This salinity values may be reached in some hypersaline chlorine-rich lakes, for which a salinity correction would be needed (Herwartz et al., 2017). Nevertheless, gypsum precipitation does not necessary occur in high-salinity environments, but often takes place in freshwater lakes saturated in calcium sulfate with relatively low salinities, often ~3-4 g/l (e.g. Hodell et al., 2005; Perez-Bielsa, 2013). The E/I of the lake has a large impact on the IMB. The E/I in modern lakes can be asserted by a simple mass balance of conservative elements in water (e.g. sodium chloride), but this parameter in the past is generally unknown. Figure 5A shows that when E/I exceeds 0.75, changes in this parameter barely affect the RH values derived from the model. We estimate the errors for the RH to be smaller than 5% (1SD) when the lake approached terminal conditions, as required for saturation in gypsum of water. In contrast, when the model is forced to E/I <0.5 the scatter of RH values increases (ca. ±15%, 1SD), suggesting that the resolution of our method for RH estimation is better for lake systems close to closed conditions (all the water loss by evaporation and practically not outflow) than for throughflow lakes. This is because of the $\delta^{18}O$-^{17}O-excess and $\delta^{18}O$ -d-excess trajectories of evaporated waters under different RH diverge considerably when E/I approaches 1 (Fig. 1). In contrast, the isotopic trajectory of water in a throughflow lake (e.g. E/I<0.5) barely differs when evaporation occurs under different conditions of RH. This indicates the method described here is especially suitable for lakes in which gypsum formed under arid or semiarid conditions (Surma et al., 2015).

In summary, when the model is forced to match both the ^{17}O-excess and d-excess of the paleo-water measured in GHW and model inputs are selected based on conservative estimates and appropriate errors, the derived uncertainty in RH can be as low as ±3% (1σ). The model is insensitive to temperature changes, whereas uncertainties in the isotopic composition of the

rainfall can have a significant effect, especially in regions where the isotopic composition of rainfall is highly variable. The accuracy of the method is best when applied to lakes under arid/semiarid climate (RH<70%) and elevated E/I (hydrologically closed basins). Most of these conditions are met for Lake Estanya where we have applied the method to estimate RH changes during the last glacial termination and Holocene.

5.3. Application to Lake Estanya

We applied the approach described above to reconstruct paleoclimate at Lake Estanya in the Southern Pyrenees during the late Glacial-Holocene transition and the Holocene. We interpret past changes in the isotopic composition in GHW of Lake Estanya in terms of changing RH (see supplementary material for detailed rationale about the environmental parameters selected for the model).

5.3.1. Bølling-Allerød period

Between ~15 and ~13 cal. kyrs BP, coinciding with the Bølling-Allerød (B-A) period, the lake showed intermediate $\delta^{18}O$ and δD values compared with the later stages. This indicates a more positive water balance compared to the subsequent period (i.e. 12.8-11.6 cal. kyrs BP; Younger Dryas). Our model based on ^{17}O-excess and d-excess suggests that RH during the B-A period was ~55-65%. This is ~10-15% less than modern conditions in the Estanya region (~70-75%). This finding is consistent with comparatively lower water salinity and greater productivity in the paleo-lake than during the YD, inferred from the elemental composition (XRF) of the sediments and $\delta^{13}C$ of organic matter, respectively (Morellón et al., 2009b) (Fig. 6). During the B-A period,

362 a trend towards heavier $\delta^{18}O$ and δD values was recorded, reaching a relative maximum at ca.
363 13.2 cal. kyrs BP, coinciding with a cold period.
364
365
366 **5.3.2. Younger Dryas**
367 Relatively enriched $\delta^{18}O$ and δD values (11.3‰ and 23.7‰, respectively) and lower d-excess (-
368 69‰) in the lake water recorded during the YD are also in good agreement with higher E/I
369 compared to previous and later stages. Accordingly, a maximum in water salinity during the YD
370 is also evidenced by the greatest contents of S and Ca^{2-} in this section of the core (XRF data in
371 Morellón et al., 2009b). The modelled ^{17}O-excess and d-excess of the paleolake water during the
372 YD indicate that atmospheric RH decreased to 40-45% during the aridity peak at ~12 cal. kyrs
373 BP. This is ~10-15% less than during the previous B-A period and ~30-35% less compared to
374 present. These values are also consistent with recent studies of biomarkes in Lake Meerfelder
375 Maar (Germany) that suggest RH decreased by 8-15% during YD compared with the previous
376 B/A period (Rach et al. 2017). Also, these results are in good agreement with previous studies
377 suggesting the YD in NE Spain was characterized by cold and arid conditions, with particularly
378 extreme conditions in higher altitudes of the Pyrenees (González-Sampériz et al., 2006).
379 Accordingly, generally drier conditions were recorded elsewhere on the Iberian Peninsula
380 (Moreno et al., 2012). A high-resolution speleothem record from El Seso Cave (Southern
381 Pyrenees) reveals a modest cooling of 1.3ºC compared with other circum-Iberian sea surface
382 temperature reconstructions (Cacho et al., 1999; Eynaud et al., 2009), and a significant decrease
383 in rainfall during the first part of the YD (12.9-12.5 cal krys BP) followed by a progressive
384 increase in humidity afterwards.

385 Drier conditions throughout the YD have also been inferred from other paleoclimatic sequences
386 in Iberia (Moreno et al., 2012, Garcia-Ruiz et al., 2016; González-Sampériz et al., 2017). The
387 maximum southward migration of the polar front during the YD reached 42ºN (Broecker et al.,
388 1988; Lane et al., 2013), approximately the latitude of the Southern Pyrenees and Lake Estanya.
389 Marine records from the Iberian Margin found a pronounced cooling during this period, even
390 more intense than in the LGM (Eynaud et al., 2009 and references therein). Furthermore, the
391 existence of loess deposits (13-10 cal. kyrs BP) in Central Spain (Bateman and Díez-Herrero,
392 2001) also supports an increase in aridity and perhaps wind speed in Western Europe during the
393 YD (Brauer et al., 2008), as suggested by our model results.
394
395 **5.3.3. Holocene**
396 The Early Holocene period (11.7 to 7.5 cal. kyrs BP) was characterized by a decrease in $\delta^{18}O$
397 and δD values (by ~9‰ and ~20‰, respectively). This indicates a more positive water balance
398 (lower E/I) compared to the YD. Our model indicates that RH increased to 50-60% during the
399 Early Holocene (~7.5-11 cal. kyrs BP). Pollen-based vegetation reconstructions indicate
400 relatively dry conditions during the transition to the Holocene marked by increasing *Juniper sp*.
401 and decreasing mesophytes (González-Sampériz et al., 2017). The isotope values reveal a
402 comparatively large increase in humidity relative to the YD, which is not reconstructed by
403 sedimentary facies and palynology but is in agreement with other paleohydrological records of
404 NE Spain and other regions from the Iberian Peninsula (Moreno et al., 2012; Morellón et al,
405 2014; González-Sampériz et al. 2017).
406 The atmospheric reorganization following the YD led to a rapid resumption of the Atlantic
407 Meridional Overturning Circulation (AMOC) and a northwards return of the polar front to 50º-

60ºN (Lane et al., 2013). This shifted the trajectory of the westerlies north to the Iberian Peninsula, and thus weakening wind intensity and increasing humidity in Southern Europe. This relative increase in moisture with respect to the previous scenario, the YD, was also reflected by a decrease in the salinity of the lake water (Fig. 6) in Estanya and by an expansion of *Juniper sp.* population in the watershed (Vegas-Vilarrubia et al., 2013; González-Sampériz et al., 2017).

During the remainder of the Holocene (7.5 to 0.6 cal. kyrs BP) the isotopic values of the lake water averaged around 4.3±0.7‰ for $\delta^{18}O$ and -1.5±2.9‰ for δD, and showed less variability than the Late Glacial owing to higher water level. The Holocene paleo-lake water values recorded by gypsum are in accordance with modern $\delta^{18}O$ and δD of the lake water, which indicates that environmental conditions were similar to present. During the Mid- Late-Holocene (7.5 cal. kyrs BP to 0.6 cal. kyrs BP), atmospheric RH stabilized around ~70%. This value is similar to the modern RH measured in the Lake Estanya region (annual mean of ~70-75%, Perez-Bielsa, 2013). These results agree with previous reconstructions based on sedimentology and geochemistry, which also show rather stable conditions similar to the present with short-lived abrupt hydrological fluctuations and an aridification trend after 4.5 to 4 cal. kyrs BP (Morellón et al., 2009b).

6. Conclusions

We propose a new proxy for quantitative estimates of paleo-humidity. Analysis of GHW permits the actual isotopic composition of paleo-waters to be determined, with little to no effect of temperature. We couple triple oxygen and hydrogen isotopes in hydration water of lacustrine gypsum and an Isotope Mass Balance model to quantify changes in RH in the past. Using Monte Carlo simulations, the RH uncertainties derived from the input parameters to our model are

estimated. This can be as low as 3% (1σ) when the model is forced to match both the ^{17}O-excess and d-excess of the paleo-water measured in GHW.

We apply this method to reconstruct the isotopic composition of paleo-waters of Lake Estanya (NE Spain) and changes in atmospheric RH over the Late Glacial and Holocene periods (from ~15 to 0.6 cal. kyrs BP). Our results indicate RH of 40-45% during the YD and increasing to 70-75% during the Mid-Late Holocene. This suggests that the mean RH in this region during the past 7.5 cal. kyr BP was similar to present (RH~75%); however, the YD was characterized by much drier conditions, with atmospheric RH ~30% lower than today. The southwards shift of the Polar Front to ca. 42ºN during the coldest phases of the YD increased wind intensity and was responsible for the minimum RH during this period.

The consistency of the results obtained from Lake Estanya with other proxies analyzed in this lake and other regional paleoclimate records, demonstrates the reliability of isotopes in gypsum hydration water as a tool for quantitative paleohydrological reconstructions in lake sediments. Improving the analytical precision of triple oxygen isotope measurements in waters and better understanding of the various parameters included in the model will reduce the uncertainties in estimated RH.

ACKNOWLEDGMENTS

This research was supported by the ERC WIHM Project (#339694) to DAH.

References

Barkan, E., Luz, B., 2005. High precision measurements of $^{17}O/^{16}O$ and $^{18}O/^{16}O$ ratios in H_2O, Rapid Commun. Mass Spectrom. 19, 3737–3742.

453 Barkan, E., Luz B., 2007. Diffusivity fractionations of $H_2{}^{16}O/H_2{}^{17}O$ and $H_2{}^{16}O/H_2{}^{18}O$ in air and
454 their implications for isotope hydrology. Rapid Commun. Mass Spectrom. 21, 2999-3005.
455 Bateman, M.D., Díez-Herrero, A., 2001. The timing and relation of aeolian sand deposition in
456 central Spain to the aeolian sand record of NW Europe. Quat. Sci. Rev. 20, 779-782.
457 Brauer, A., Haug, G.H., Dulski, P., Sigman, D.M., Negendank, J.F.W., 2008. An abrupt wind
458 shift in western Europe at the onset of the Younger Dryas cold period. Nature Geosci. 1, 520-
459 523.
460 Broecker, W.S., Andree, M., Wolfli, W., Oeschger, H., Bonani, G., Kennett, J., Peteet, D., 1988.
461 The chronology of the last Deglaciation: Implications to the cause of the Younger Dryas
462 Event. Paleoceanography 3, 1-19.
463 Cacho, I., Grimalt, J.O., Pelejero, C., Canals, M., Sierro, F.J., Flores, J.A., Shackleton, N., 1999.
464 Dansgaard-Oeschger and Heinrich event imprints in Alboran Sea paleotemperatures.
465 Paleoceanography 14, 698-705.
466 Criss, R.E., 1999. Principles of Stable Isotope Distribution, Oxford Univ. Press, Oxford, U. K.
467 Dongmann, G., Nürnberg, H.W., Förstel, H., Wagener, K., 1974. On the Enrichment of $H_2{}^{18}O$ in
468 the Leaves of Transpiring Plants. Rad. and Environm. Biophys. 11, 41–52.
469 Escobar, J., Hodell, D. A., Brenner, M., Curtis, J. H., Gilli, A., Mueller, A. D., Anselmetti, F. S.,
470 Ariztegui, D., Grzesik, D.A., Pérez, L., Schwalb, A., Guilderson, T.P., 2012. A ~43-ka record
471 of paleoenvironmental change in the Central American lowlands inferred from stable isotopes
472 of lacustrine ostracods. Quat. Sci. Rev. 37, 92–104,
473 Evans, N.P., Turchyn, A., Gázquez, F., Bontognali, T.R.R., Chapman, H., Hodell, D., 2015.
474 Coupled measurements of $\delta^{18}O$ and δD of hydration water and salinity of fluid inclusions in

gypsum from the Messinian Yesares member, Sorbas Basin (SE Spain). Earth Planet. Sci. Lett. 430, 499-510.

Eynaud, F., de Abreu, L., Voelker, A., Schönfeld, J., Salgueiro, E., Turon, J.-L., Penaud, A., Toucanne, S., Naughton, F., Sánchez-Goñi, M.F., Malaizé, B., Cacho, I., 2009. Position of the Polar Front along the western Iberian margin during key cold episodes of the last 45 ka. Geochem., Geophy., Geosys. 10, Q07U05.

Fontes, J.C., Gonfiantini, R., 1967. Fractionnement isotopique de l'hydrogène dans l'eau de cristallistion du gypse. Cr. Acad. Sci. d. Nat. 265, 4-6.

Frigola, J., Moreno, A., Cacho, I., Canals, M., Sierro, F.J., Flores, J.A., Grimalt, J.O., 2008. Evidence of abrupt changes in Western Mediterranean Deep Water circulation during the last 50 kyr: a high-resolution marine record from the Balearic Sea. Quat. Int. 181 (1), 88–104.

García-Ruiz, J.M., Palacios, D., González-Sampériz, P., de Andrés, N., Moreno, A., Valero-Garcés, B., Gómez-Villar, A., 2016. Mountain glacier evolution in the Iberian Peninsula during the Younger Dryas. Quat. Sci. Rev. 138, 16–30.

Gázquez, F., Mather, I., Rolfe, J., Evans, N.P., Herwartz, D., Staubwasser, M. Hodell D.A., 2015. Simultaneous analysis of $^{17}O/^{16}O$, $^{18}O/^{16}O$ and $^{2}H/^{1}H$ of gypsum hydration water by cavity ringdown laser spectroscopy. Rapid Commun. Mass Spectrom. 21, 1997-2006.

Gázquez, F., Evans, N.P., David. A. Hodell 2017a. Precise and accurate isotope fractionation factors ($\alpha^{17}O$, $\alpha^{18}O$ and αD) for water and $CaSO_4 \cdot 2H_2O$ (gypsum). Geochim. Cosmochim. Acta, 198, 259-270.

Gázquez, F., Calaforra, J.M., Evans, N.P., David. A. Hodell 2017b. Using stable isotopes ($\delta^{17}O$, $\delta^{18}O$ and δD) of gypsum hydration water to ascertain the role of water condensation in the formation of subaerial gypsum speleothems. Chem. Geol. 452, 34-46.

Gibson, J.J., Birks, S.J., Yi, Y., 2016. Stable isotope mass balance of lakes: a contemporary perspective. Quat. Sci. Rev. 131, 316-328.

Gonfiantini, R., Fontes, J.C., 1963. Oxygen isotopic fractionation in the water of crystallization of gypsum. Nature 200, 644-646.

González-Sampériz, P., Valero-Garcés, B.L., Moreno, A., Jalut, G., García-Ruiz, J.M., Martí-Bono, C., Delgado-Huertas, A., Navas, A., Otto, T., Dedoubat, J.J., 2006. Climate variability in the Spanish Pyrenees during the last 30,000 yr revealed by the El Portalet sequence. Quat. Res. 66, 38-52.

González-Sampériz, P., Aranbarri, J., Pérez-Sanz, A., Gil-Romera, G., Moreno, A., Leunda, M., Sevilla-Callejo, M., Corella, J.P., Morellón, M., Oliva, B., Valero-Garcés, B., 2017. Environmental and climate change in the southern Central Pyrenees since the Last Glacial Maximum: A view from the lake records. Catena 149(3), 668-688.

Grauel, A.L., Hodell, D., Bernasconi, S.F., 2016. Quantitative estimates of tropical temperature change in lowland Central America during the last 42 ka. Earth Planet. Sci. Lett. 438, 37-46.

Jasechko, S., Lechler, A., Pausata, F.S.R., Fawcett, P. J., Gleeson, T., Cendón, D. I., Galewsky, J., LeGrande, A. N., Risi, C., Sharp, Z. D., Welker, J. M., Werner, M. and Yoshimura. K., 2015. Late-glacial to late-Holocene shifts in global precipitation $\delta^{18}O$. Clim. Past 11, 1375-1393.

Haese, B., Werner, M., Lohmann, G., 2013. Stable water isotopes in the coupled atmosphere-land surface model ECHAM5-JSBACH. Geosci. Model Dev. 6, 1463–1480.

Herwartz, D., Surma, J., Voigt, C., Assonov, S., Staubwasser, M., 2017. Triple oxygen isotope systematics of structurally bonded water in gypsum. Geochim. Cosmochim. Acta 209: 254-266.

Hodell, D.A, Curtis, J.H., Brenner, M., 1995. Possible role of climate in the collapse of Classic Maya civilization. Nature 375, 391–394.

Hodell, D.A., Benner, M., Curtis, J.H., 2005. Terminal Classic drought in the northern Maya lowlands inferred from multiple sediment cores in Lake Chichancanab (Mexico). Quat. Sci. Rev. 24, 1413–1427.

Hodell, D., Turchyn, A.V., Wiseman, C.J., Escobar, J., Curtis, J.H., Brenner, M., Gilli, A. Mueller, A.D., Anselmetti, F., Aritzegui, D., Brown, E., 2012. Late Glacial temperature and precipitation changes in the lowland Neotropics by tandem measurement of $\delta^{18}O$ in biogenic carbonate and gypsum hydration water. Geochim. Cosmochim. Acta 77, 352-368.

Kathayat, G., Cheng, H., Sinha, A., Spötl, C., R. Edwards, L., Li, H.Z., Yi, X., L., Ning, Y., Cai, Y., Weiguo, L.L, Breitenbach, S.F.M., 2016. Indian monsoon variability on millennial-orbital timescales. Sci. Rep. 6, 24374.

Landais, A., Barkan, E., Yakir, D., Luz, B., 2006. The triple isotopic composition of oxygen in leaf water. Geochim. Cosmochim. Acta 70, 4105–4115.

Lane, C.S., Brauer, A., Blockley, S.P.E., Dulski, P., 2013. Volcanic ash reveals time-transgressive abrupt climate change during the Younger Dryas. Geology 41, 1251-1254.

Li, J., Li, M., Fang, X., Zhang, G., Zhang, W., Liu, X., 2017. Isotopic composition of gypsum hydration water in deep Core SG-1, western Qaidam basin (NE Tibetan Plateau), implications for paleoclimatic evolution. Global Planet Change. 155, 70-77.

Luz, B., Barkan E., 2010. Variations of $^{17}O/^{16}O$ and $^{18}O/^{16}O$ in meteoric waters. Geochim. Cosmochim. Acta 74, 6276–6286.

Morellón, M., Valero-Garcés, B., Anselmetti, F., Ariztegui, D., Schnellmann, M., Moreno, A., Mata, P., Rico, M., Corella, J.P., 2009a. Late Quaternary deposition and facies model for karstic Lake Estanya (North-eastern Spain). Sedimentology 56, 1505-1534.

Morellón, M., Valero-Garcés, B., Vegas-Vilarrúbia, T., González-Sampériz, P., Romero, Ó., Delgado-Huertas, A., Mata, P., Moreno, A., Rico, M., Corella, J.P., 2009b. Lateglacial and Holocene palaeohydrology in the western Mediterranean region: The Lake Estanya record (NE Spain). Quat. Sci. Rev. 28, 2582-2599.

Morellón, M., Valero-Garcés, B., González-Sampériz, P., Vegas-Vilarrúbia, T., Rubio, E., Rieradevall, M., Delgado-Huertas, A., Mata, P., Romero, Ó., Engstrom, D., López-Vicente, M., Navas, A., Soto, J., 2011. Climate changes and human activities recorded in the sediments of Lake Estanya (NE Spain) during the Medieval Warm Period and Little Ice Age. J. Paleolimnol. 46, 423-452.

Morellón, M., Benito, G., Moreno, A., González-Sampériz, P., Sánchez-Moya, Y., Pérez-Sanz, A., Mata, P., Aranbarri, J., Sopeña, A., Valero-Garcés, B., 2014. Hydrological response to the GS-1/Holocene transition in the Iberian Peninsula: environmental leads and lags, COST INTIMATE MC Final workshop, Zaragoza (Spain).

Moreno, A., Gonzalez-Samperiz, P., Morellón, M., Valero-Garces, B.L., Fletcher, W.J., 2012a. Northern Iberian abrupt climate change dynamics during the last glacial cycle: A view from lacustrine sediments. Quat. Sci. Rev. 36, 139-153.

Ortiz, J.E., Torres, T., Delgado, A., Reyes, E., Llamas, J.F., Soler, V., Raya, J., 2006. Pleistocene paleoenvironmental evolution at continental middle latitude inferred from carbon and oxygen stable isotope analysis of ostracodes from the Guadix-Baza Basin (Granada, SE Spain). Palaeogeogr. Palaeoclimatol. Palaeoecol. 240, 536–561.

564 Passey, B.H., Hu, H, Ji, H., Montanari, S., Li, S., Henkes, G.A., Levin, N.E. 2014. Triple oxygen
565 isotopes in biogenic and sedimentary carbonates. Geochim. Cosmochim. Acta 141,1–25.
566 Perez-Bielsa, C. 2013. Funcionamiento hidrogeológico de un humedal hipogenioco de origen
567 kárstico en las sierras marginas pirenaicas: Las lagunas de Estaña (Huesca). PhD Thesis.
568 Madrid, 419 pp.
569 Rach, O., Kahmen, A., Brauer, A., Sachse, D. 2017. A dual-biomarker appoach for
570 quantification of changes in relative humidity from sedimentary lipid D/H ratios. Clim. Past
571 Discuss. doi:10.5194/cp-2017-7.
572 Rasmussen, S.O., Seierstad, I.K., Andersen, K.K., Bigler, M., Dahl-Jensen, D., Johnsen, S.J.,
573 2008. Synchronization of the NGRIP, GRIP, and GISP2 ice cores across MIS 2 and
574 palaeoclimatic implications. Quat. Sci. Rev., 27, 18-28.
575 Schoenemann, S.W., Schauer, A. J., Steig E. J. 2013. Measurement of SLAP and GISP $\delta^{17}O$ and
576 proposed VSMOW-SLAP normalization for ^{17}O-excess. Rapid Commun. Mass Spec. 27,
577 582–590.
578 Sofer Z.,Gat J.R., 1975. The lsotopic composition of evaporating brines: effect of the isotopic
579 activity ratio in saline solutions. Earth Planet. Sci. Lett. 26, 179-186.
580 Steig, E.J., Gkinis, V., Schauer, A.J., Schoenemann, S.W., Samek, K., Hoffnagle, J., Dennis,
581 K.J., Tan, S.M., 2014. Calibrated high-precision ^{17}O-excess measurements using laser-current
582 tuned cavity ring-down spectroscopy, Atmos. Meas. Tech. 7, 2421-2435.
583 Surma, J., Assonov, S., Bolourchi, M.J., Staubwasser, M., 2015. Triple oxygen isotope
584 signatures in evaporated water bodies from the Sistan Oasis, Iran. Geophys. Res. Lett., 42,
585 8456–8462.

Torfstein, A., Gavrieli, I., Katz, A., Kolodny, Y., Stein, M., 2008. Gypsum as a monitor of the paleo-limnological-hydrological conditions in Lake Lisan and the Dead Sea. Geochim. Cosmochim., 72, 2491-2509.

Uemera, R., Barkan, E., Abe, O., Luz, B., 2010. Triple isotope composition of oxygen in atmospheric water vapor. Geophys. Res. Lett. 37, L04402, doi:10.1029/2009GL041960.

Valero-Garcés, B., Morellón, M., Moreno, A., Corella, J.P., Martín-Puertas, C., Barreiro, F., Pérez, A., Giralt, S., Mata-Campo, M.P., 2014. Lacustrine carbonates of Iberian Karst Lakes: Sources, processes and depositional environments. Sedim. Geol. 299, 1-29.

Vegas-Vilarrúbia, T., González-Sampériz, P., Morellón, M., Gil-Romera, G., Pérez-Sanz, A., Valero-Garcés, B., 2013. Diatom and vegetation responses to Late Glacial and Early Holocene climate changes at Lake Estanya (Southern Pyrenees, NE Spain). Palaeogeogr., Palaeoclimatol, Palaeoecol. 392, 335-349.

FIGURE CAPTIONS

Figure 1. Sensitivity of $\delta^{18}O$-^{17}O-excess and $\delta^{18}O$-d-excess to different environmental parameters during evaporation of a water body ($\delta^{18}O$=-8‰, δD=-54‰, ^{17}O-excess=30 per meg and d-excess=10‰) in partial equilibrium with atmospheric vapor. The isotopic composition of a terminal lake has been model under different conditions of relative humidity (A and F), temperature (B and G), wind (C and H) and degree of equilibrium between the atmospheric vapor and the freshwater member (D and I). The isotopic compositions of water pools with different ratios of Evaporation/Inflow (E/I), keeping the rest of parameter constant, are also represented (E and J).

Fig. 2. A. Location of Lake Estanya. The red dashed line indicates the limits of the surface catchment. Coring sites in Estanque Pequeño de Abajo are labelled.

Fig. 3. $\delta^{18}O$ and δD of rain and spring waters (green triangles), modern water from Lake Estanya (red diamonds), and gypsum hydration waters (unfilled blue circles) ranging in age from 14.7 to 0.6 cal. kyrs BP. The isotopic values of paleo-lake waters (filled blue circles) were inferred using isotopic fractionation factors between gypsum hydration water and the free solution (Gázquez et al., 2017a).

Fig. 4. Results of the IMB model experiments (A. $\delta^{18}O$ vs. ^{17}O-excess; B. $\delta^{18}O$ vs. d-excess). The colored diamonds represent the isotopic composition of Lake Estanya during the Holocene (yellow), Preboreal (green), Younger Dryas (blue) and the Bølling-Allerød (pink) periods. The model (blue lines and black dots) is tuned to fit the gypsum mother water compositions. Environmental conditions for the different periods were simulated using the input parameters in Table 1. The grey ellipses represent the uncertainty in the model derived from the tolerance given for each input parameter.

Fig 5. Sensitivity experiments of the derived relative humidity to other major variables: Evaporation/Input and the isotopic composition of the input. In both experiments data points representative of the late-Holocene (blue markers) and the Younger Dryas (red markers) are used to illustrate the potential biases in the derived relative humidity estimates: **A.** The derived relative humidity shows a strong positive correlation to the assumed E/I in the range of 0.4-0.7 and the effect is greater at lower relative humidities (e.g. the YD). The effect is much weaker at higher E/I in closed lake basins, such as Lake Estanya (as well as most other systems in which

632 evaporite mineral precipitation occurs); **B.** The derived relatively humidity with respect to the
633 assumed isotopic composition of the freshwater input. Here, relatively humidity shows a small
634 positive relationship with the isotopic composition of the freshwater input, which translates into
635 an error of between 3-4.6% in relative humidity for every 1‰ change in the freshwater water
636 input.
637
638 **Fig. 6** Isotopic composition of Lake Estanya water, reconstructed atmospheric RH during the
639 Late Glacial-Holocene transition and the Holocene and comparison with other global and
640 regional paleoclimatic archives, including, from top to bottom: 1) NGRIP $\delta^{18}O$ (Rasmussen et
641 al., 2008), 2) winter (blue line) and summer (red line) insolation at 42ºN, 3) Si/Al record in
642 marine core MD99-2343, offshore Minorca (Frigola et al, 2008); 4) Alboran Sea core MD95-
643 2043 Sea Surface Temperature (SST) (Cacho et al., 1999); the isotopic composition of the paleo-
644 lake water reconstructed from gypsum hydration water (panels 5, 6 and 7); 8) atmospheric RH
645 obtained from our ^{17}O-excess/d-excess model. The mean RH obtained from the ^{17}O-excess
646 model are represented as diamonds (see Fig. 4A). The RH results of the Monte Carlo simulation
647 in two scenarios are represented by the color shading. Scenario 1 (blue banding) in which all the
648 model parameters are held constant for all time periods and scenario 2 (orange banding) in which
649 the model parameters are modified in the Younger Dryas as described in the main text and
650 shown in Table 1. Previous palaeoenvironmental reconstruction of Lake Estanya based on
651 sedimentological and geochemical proxies, including 9) $\delta^{13}C$ in organic matter, 10) a paleo-
652 salinity proxy obtained from XRF analyses of the sedimentary sequence and, 11) relative lake
653 level reconstruction (0-10 stages) based on sedimentary facies (Morellón et al., 2009b).
654

Figure 1

Click here to download high resolution image

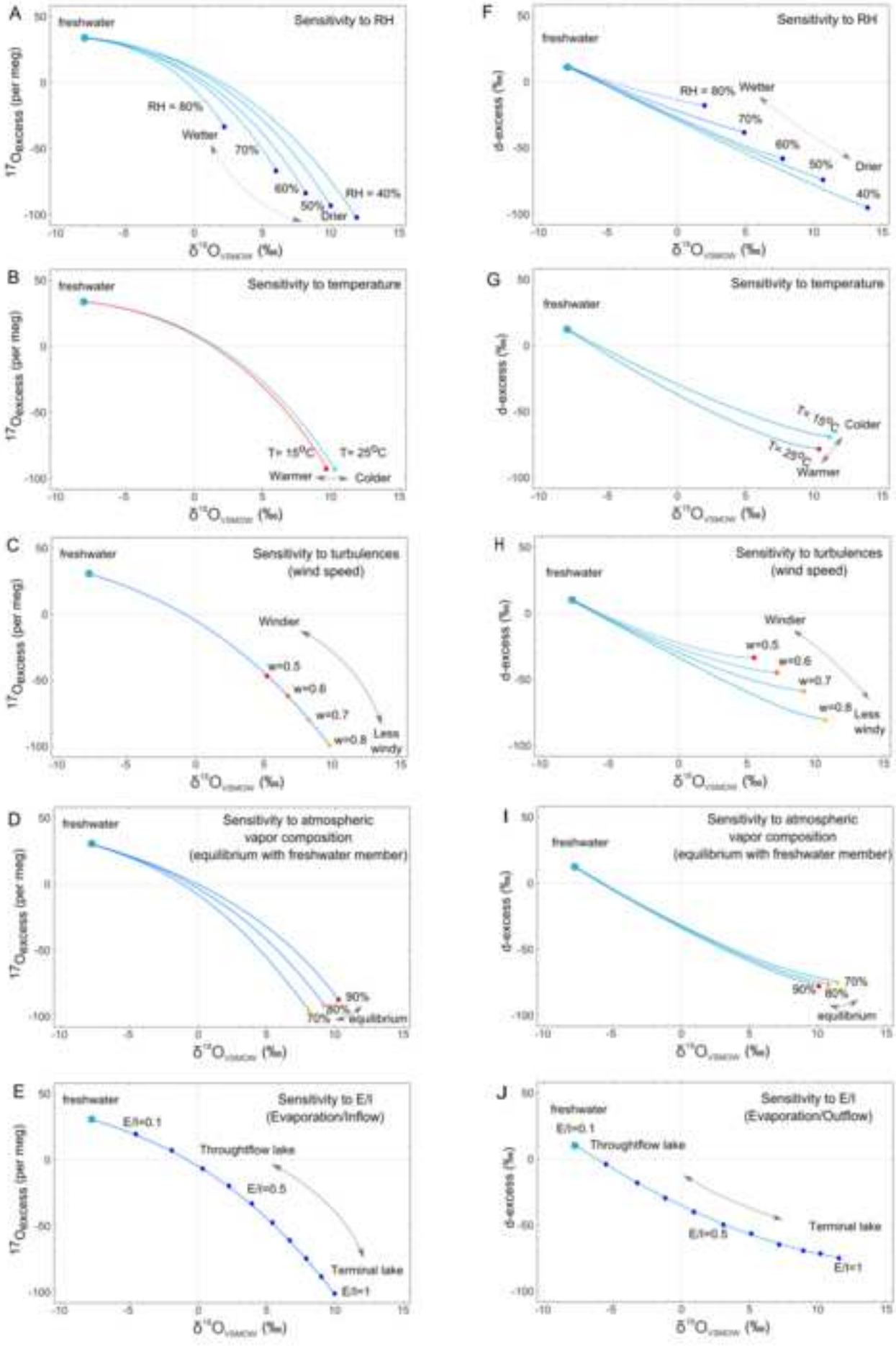

Figure 2

Click here to download high resolution image

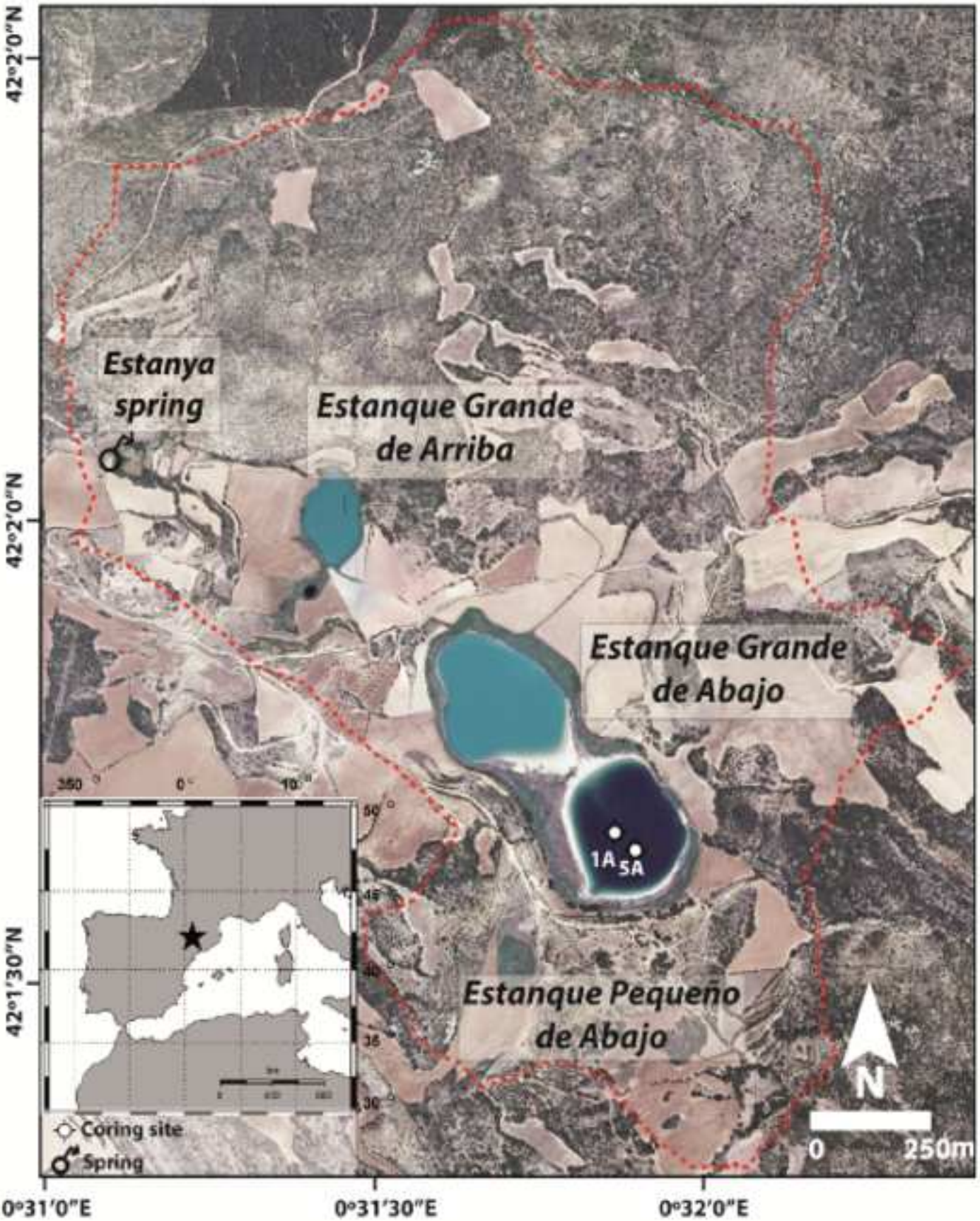

Figure 3

Click here to download high resolution image

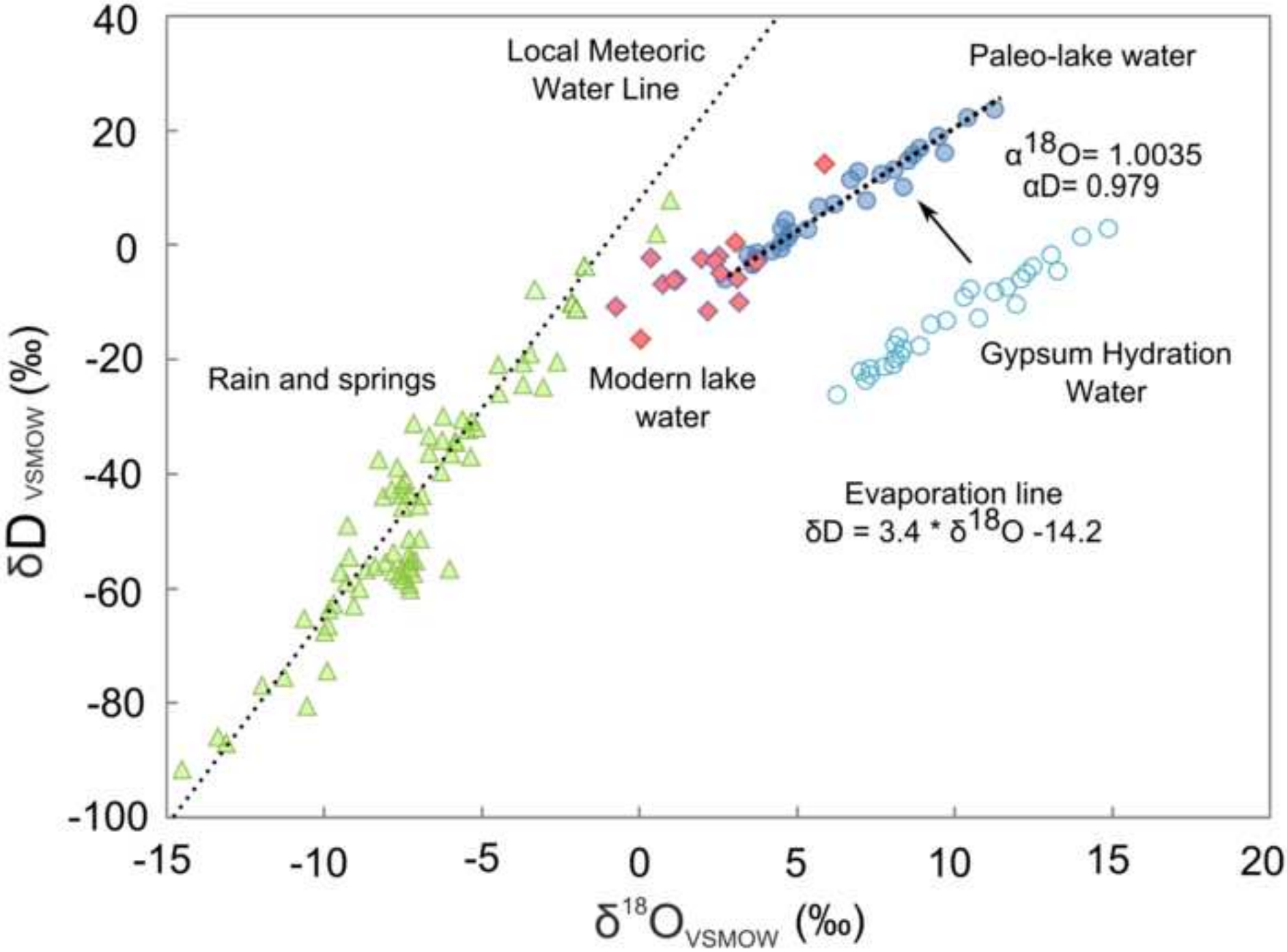

Figure 4

Click here to download high resolution image

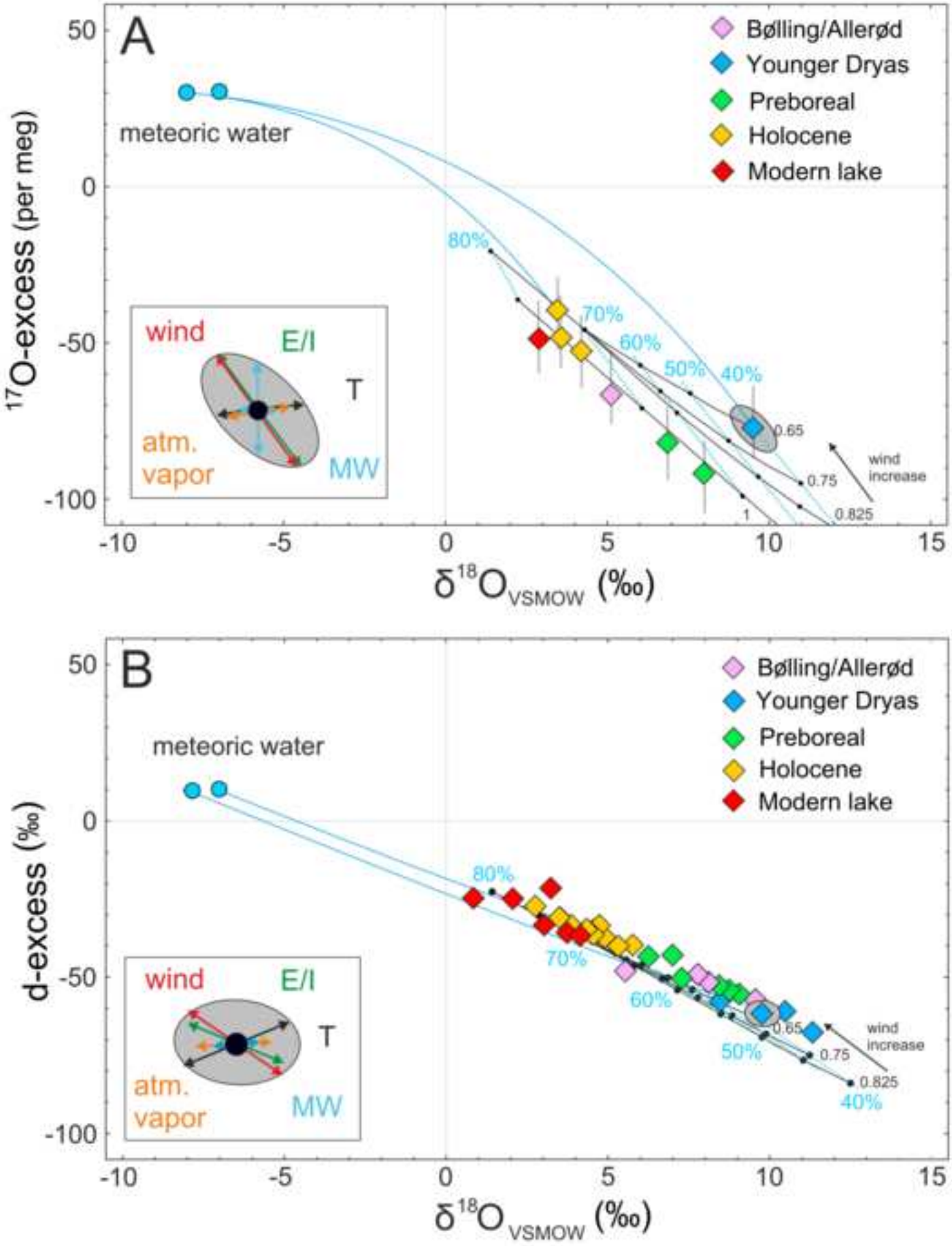

Figure 5

Click here to download high resolution image

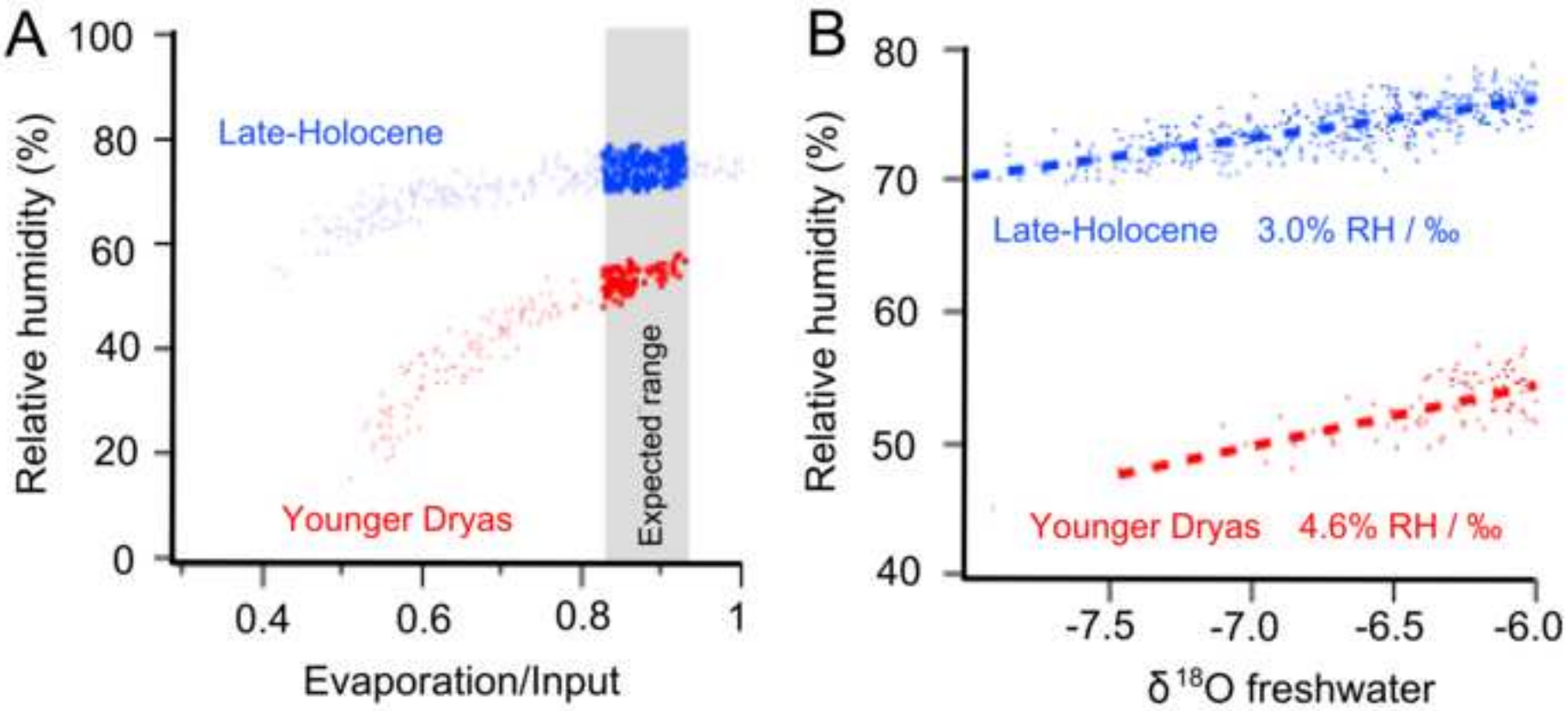

Figure 6

Click here to download high resolution image

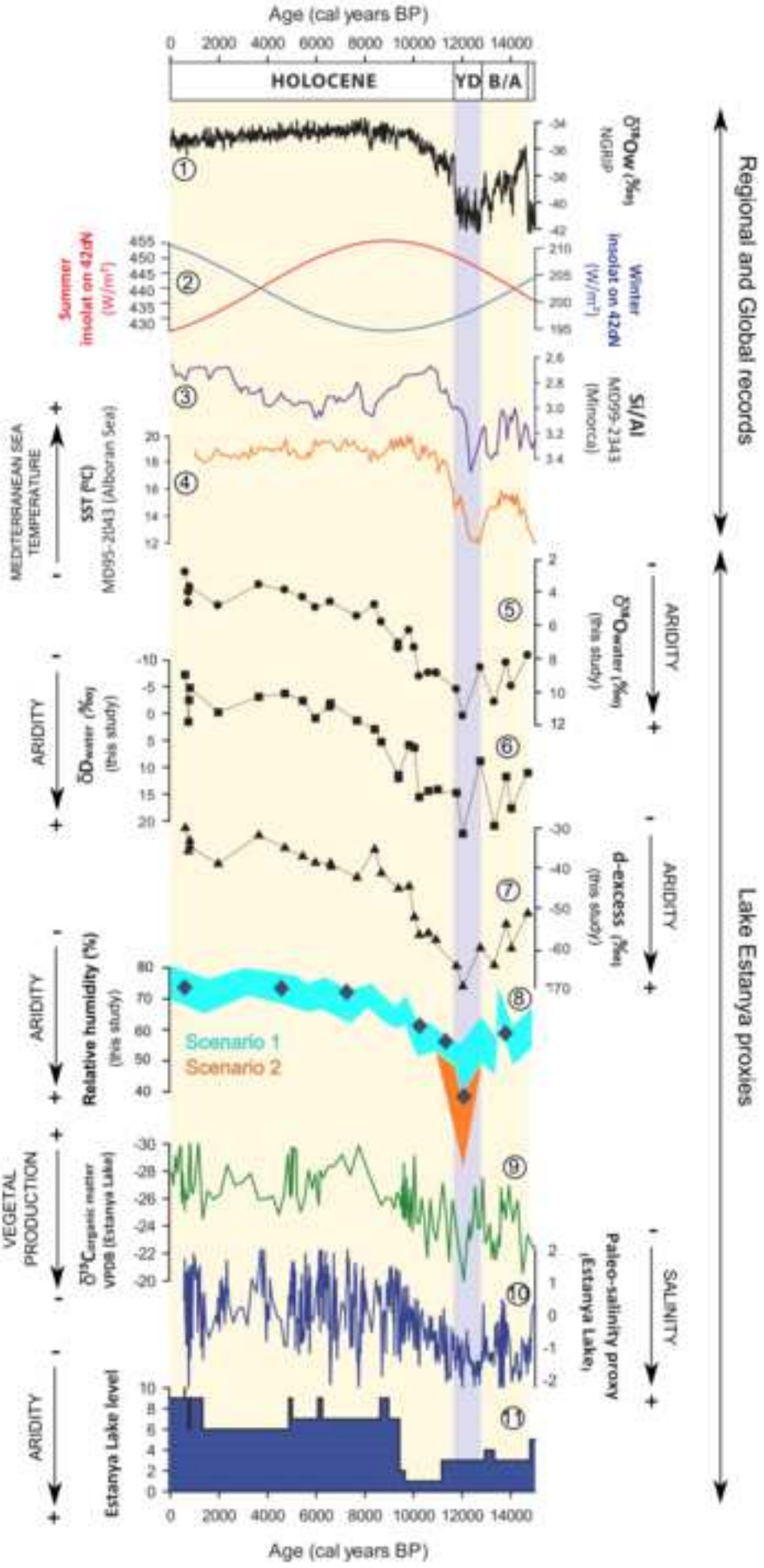

Supplementary material for online publication only

Click here to download Supplementary material for online publication only: Supplementary material v. final 14-07-17.docx